[8] Landahl, M. T., "On the stability of a laminar incompressible boundary layer over a flexible surface," J. Fluid Mech. **13**, 609–632 (1962).

[9] Benjamin, T. B., "The threefold classification of unstable disturbances in flexible surfaces bounding inviscid flows," J. Fluid Mech. **16**, 436–450 (1963).

[10] Dugundji, J., Dowell, E., and Perkin, B., "Subsonic flutter of panels on continuous elastic foundations—experiment and theory," Massachusetts Institute of Technology Aeroelastic and Structures Research Lab. TR 74-4 (April 1962).

[11] Kevorkian, J., "The two variable expansion procedure for the approximate solution of certain non-linear differential equations," Rept. SM-42620, Missile and Space Systems Div., Douglas Aircraft Co., Santa Monica, Calif. (1962).

[12] Kelly, R. E., "The stability of an unsteady Kelvin-Helmholtz flow," J. Fluid Mech. (to be published).

JUNE 1965 AIAA JOURNAL VOL. 3, NO. 6

Elastic Stability of Thin-Walled Cylindrical and Conical Shells under Combined Internal Pressure and Axial Compression

V. I. WEINGARTEN*
University of Southern California, Los Angeles, Calif.

E. J. MORGAN†
Aerojet-General Corporation, Azusa, Calif.

AND

PAUL SEIDE‡
Aerospace Corporation, El Segundo, Calif.

The results of an extensive experimental program on the stability of cylindrical and conical shells under internal pressure and axial compression are presented. The use of the given data for design criteria is discussed, and recommendations are given. The experimental data for elastic, pressurized cylinders under axial compression indicated that the load carried by the cylinder in addition to that carried by internal pressure increases to the value given by small-deflection theory for unpressurized cylinders. The variation of the net load with internal pressure was found to depend on the radius-thickness ratio of the cylinder, and curves suitable for design were obtained. Experimental buckling loads obtained for conical shells were in good agreement with small-deflection theory predictions for sufficiently high pressures. The results indicated that the end-support condition may be more important for cones than cylinders. Insufficient data were obtained, however, to enable design curves to be recommended in the low-pressure region.

Nomenclature

E = Young's modulus of shell wall material
L = axial length of cylinder or cone
P = total axial load at buckling
p = uniform internal or external hydrostatic pressure
$\bar{p}$ = internal pressure parameter $\{p[(R_1/\cos\alpha)/t]^2/E$ for cones or $p/E(R/t)^2$ for cylinders$\}$
$\tilde{p}$ = $p/E(R/t)^{5/3}$
R = cylinder radius
R_1 = radius of small end of cone
t = shell wall thickness
Z = cylinder curvature parameter $[3(1-\nu^2)]^{1/2}L^2/Rt$
α = semivertex angle of cone
δ_{cr} = critical load shortening parameter $[(\Delta L_{cr}/L)R/t]$
γ = internal pressure parameter $\{[3(1-\nu^2)/2]^{1/2}(p/E) \times [(R_1/\cos\alpha)/t]^2\}$
ϵ/ϵ_{cl} = ratio of compressive strain and classical buckling strain
ν = Poisson's ratio of wall material
σ, σ_{cr} = critical average compressive stress $P_{cr}/2\pi Rt$
$\bar{\sigma}_{cr}$ = critical average compressive stress coefficient $[\sigma_{cr}/(Et/R)]$
σ_c, σ_c = theoretical compressive buckling stress $\{E/[3(1-\nu^2)]^{1/2}(t/R)\}$
$\bar{\sigma}_{prop\ limit}$ = stress coefficient at proportional limit of material $[\sigma_{prop\ limit}/(Et/R)]$
σ_{min} = minimum axial compressive stress in buckled state
$\bar{\sigma}_{min}$ = minimum axial compressive stress coefficient $\{\sigma_{min}/[E(t/R)]\}$
ΔL_{cr} = total end shortening at buckling
ζ = cone geometry parameter $\{[12(1-\nu^2)]^{1/2} \times [(R_1/\cos\alpha)/t]\cot^2\alpha\}$

Received August 4, 1964; revision received February 9, 1965. The work contained in this paper was performed at Space Technology Laboratories, Inc. under Contract No. AF 04(657)-619.

* Assistant Professor, Civil Engineering. Member AIAA.

† Head, Aerospace Tankage Structures Support Section. Member AIAA.

‡ Staff Scientist. Associate Fellow Member AIAA.

Introduction

INCREASED emphasis has recently been placed upon the internally pressurized monocoque cylinders and cones as an efficient load carrying structure for missile applications. As a result, several experimental investigations have been reported in the literature.[1–5] Practically all the results obtained to date for cylindrical shells seem inconsistent with current explanations of cylinder behavior. With the exception of the study of Ref. 1, even large amounts of internal pressure did not stabilize the test cylinders to the extent that the theoretical

small-deflection buckling stress was achieved. Although the discrepancy between theory and experiment is usually attributed to geometric imperfections and associated stress concentrations, large values of internal pressure should remove these initial imperfections and provide cylinders that are substantially perfect. In most cases, it is suspected that the plastic yielding of the material, whether a result of high buckling stresses or excessive initial damage, is the cause of the current confusion of the results.

In order to provide test data on pressurized unstiffened cylinders and cones that would be less sensitive to plasticity effects, tests were made on shells constructed of Mylar. The results of this investigation are reported herein.

Specimen Fabrication

The specimens used in the experiments were made of Mylar polyester sheet. This has been found to have a Young's modulus of 700,000 psi, a Poisson's ratio of 0.3, and proportional limit and yield stresses of 6000 and 11,000 psi, respectively. Because of the small variation of the properties of Mylar from roll to roll, the modulus of elasticity was determined by using a load-deflection curve for each specimen.

Specimens were made by cutting accurately developed cones and cylinders from the Mylar sheet, allowing $\frac{1}{2}$ in. on the top, a minimum of $\frac{3}{4}$ in. on the bottom for clamping, and $\frac{3}{4}$ in. overlap for the longitudinal seam. All the cones were made with the same base radius to reduce the number of base clamping fixtures needed. The developed cone was then wrapped firmly about a conical wooden mandrel. A lap joint fastened with double-backed adhesive cellophane tape was used for the longitudinal seam. In later tests, the bonding material was changed to Eccobond, an epoxy cement, after experimentation with various bonding agents. Although the thin Mylar sheet is quite flexible, the use of carefully laid out patterns and conical assembly mandrels made it possible to obtain specimens that were dimensionally accurate and relatively free of initial wrinkles or bulges. The specimens were attached to end caps by casting the specimen edges into circular end grooves filled with a low-melting-point alloy. A detailed discussion of the specimen fabrication technique is given in Ref. 6.

Test Apparatus and Procedure for Cylindrical Shells

The setup for the compression tests is shown in the photograph of Fig. 1. The test specimen assembly is illustrated in Fig. 2. The specimens were of 8-in. length and 8-in. diam. To maintain concentricity of the cylinders during casting, the grooves in the end caps were stepped to provide a locating diameter. The alignment of the two caps during assembly was provided by the center post and ball bushing assembly. The tolerance between post and bushing was adjusted to eliminate friction and to permit freedom of rotation during the tests.

It was necessary to counterbalance the top cap weight, and very careful specimen installation was required to avoid initial wrinkling of the 2- and 3-mil cylinders. The center post of the top cap also provided a mounting for a differential transformer. This displacement transducer permitted measurement of the relative movement between the caps along the axis of the cylinder. Pressurization of the cylinders was accomplished with compressed air through ports in the bottom cap. An accumulator in series with the specimen increased the control volume and assisted in stabilizing the air pressure. The compressive load was applied with a motorized screw mechanism in series with a Statham load cell, a ball bearing, and a cover plate as illustrated in Fig. 2. The floating cover plate provided clearance for the transducer leads and eliminated deflections of the top cap from the transducer's measurements. Throughout the testing, the loading mechanism provided a uniform strain rate of approximately 0.4%/min.

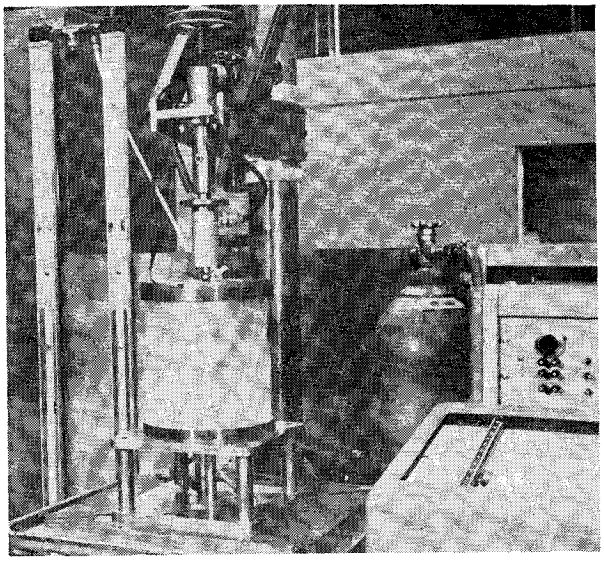

Fig. 1 Test setup for internally pressurized cylinders in axial compression.

Load and deformation were recorded simultaneously with a Mosley X-Y recorder. The internal pressure was measured by manometers.

For each fixed pressure, the axial load was gradually increased until snap buckling occurred or until an ultimate load was reached. Then the load was decreased until the buckles disappeared. Load-deflection diagrams were recorded continuously during the loading and unloading process. The internal pressure was then increased a given amount and the process repeated. After the maximum pressure was reached, a rerun was made at zero pressure to determine the degree of deterioration of the specimen.

Load-Deflection Characteristics for Cylindrical Shells

A set of typical load-deflection diagrams for various pressures is presented in Fig. 3. The occurrence of diamond-shaped buckles was unmistakable, since they appeared with a snapping noise. In the diagrams, this phenomenon is illustrated by the sharpness of the load drop-off and by the size of the unloading hysteresis loop. For increased internal pressure, buckling occurred with a smaller and elongated diamond pattern. In the figure, this change is illustrated by a decrease in the load drop-off and by a reduction in the size of the hysteresis loop.

At the higher values of $\bar{p}$, initial circumferential ripples resembling the sinusoidal waves, assumed in the classical small-

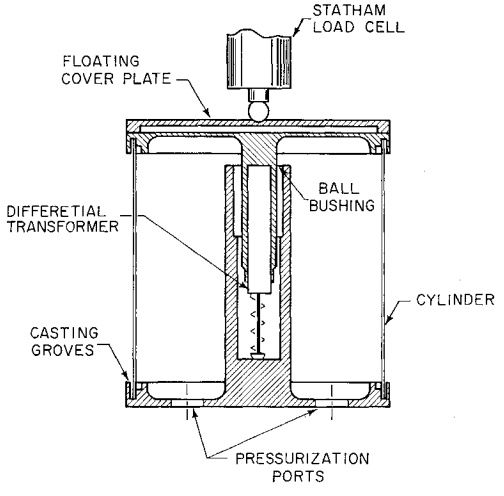

Fig. 2 Test specimen assembly.

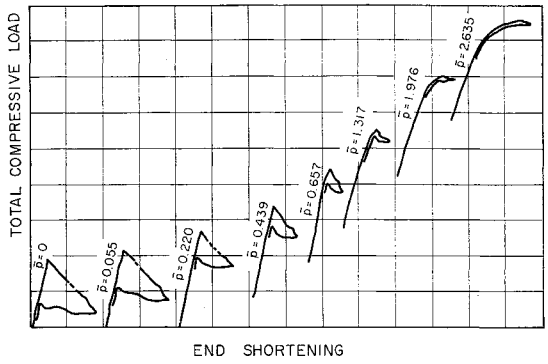

Fig. 3 Typical load-deflection curves for pressurized cylinders in axial compression.

deflection theory, appeared prior to collapse. The occurrence of these ripples is illustrated by the gradual change in the slope of the load-deformation wave.

Generally, these ring-shaped deformations appeared near the end caps. For the thinner cylinders, increased compressive load caused these waves to grow and to propagate from the ends, until they extended over the entire length of the cylinder. Then elongated diamonds developed in the waves near the ends, and the load dropped off gradually. It is interesting to note that this behavior is in qualitative agreement with the predictions of the large-deflection theory of Ref. 7. For the thicker cylinders, however, these waves were confined to the region near the ends. When the compressive load was increased, the central portion of the cylinders remained undeformed, whereas the end waves grew until either diamond-shaped buckles developed or the cylinder ends became plastic, when the load decreased slowly.

Although the shape of the loading portion of the diagrams did not change, the onset of plasticity was readily recognized. In addition to a decrease in the net collapse load, the unloading portion of the diagrams changed. Instead of dropping to a minimum and then recovering slightly as the diamond-shaped buckles disappeared, the load dropped continuously. The diagrams for high pressures in Fig. 3 illustrate this trend. The cylinder appears to have lost its ability to recover, and, as it becomes more plastic, this inability increases.

Measured load-end shortening curves for the test cylinders are illustrated in Fig. 4. The test results for three values of $\bar{p}$ are compared with the theoretical curves derived by Dow and Peterson[8] for finite cylinders with axisymmetric deformation. As indicated by the theory, the deviation from the unit slope curve of unpressurized, unrestrained cylinders increases with decreasing values of the curvature parameter and with increasing values of the pressure parameter. For the higher values of Z (lower values of thickness), the agreement between theory and experiment is excellent, even at high values of $\bar{p}$. But for the two thicker cylinders, the deviation from the unit slope is even greater than predicted by theory. This deviation of the experimental load-shortening curves from theory is apparently associated with the difference of the radial deformation pattern previously discussed.

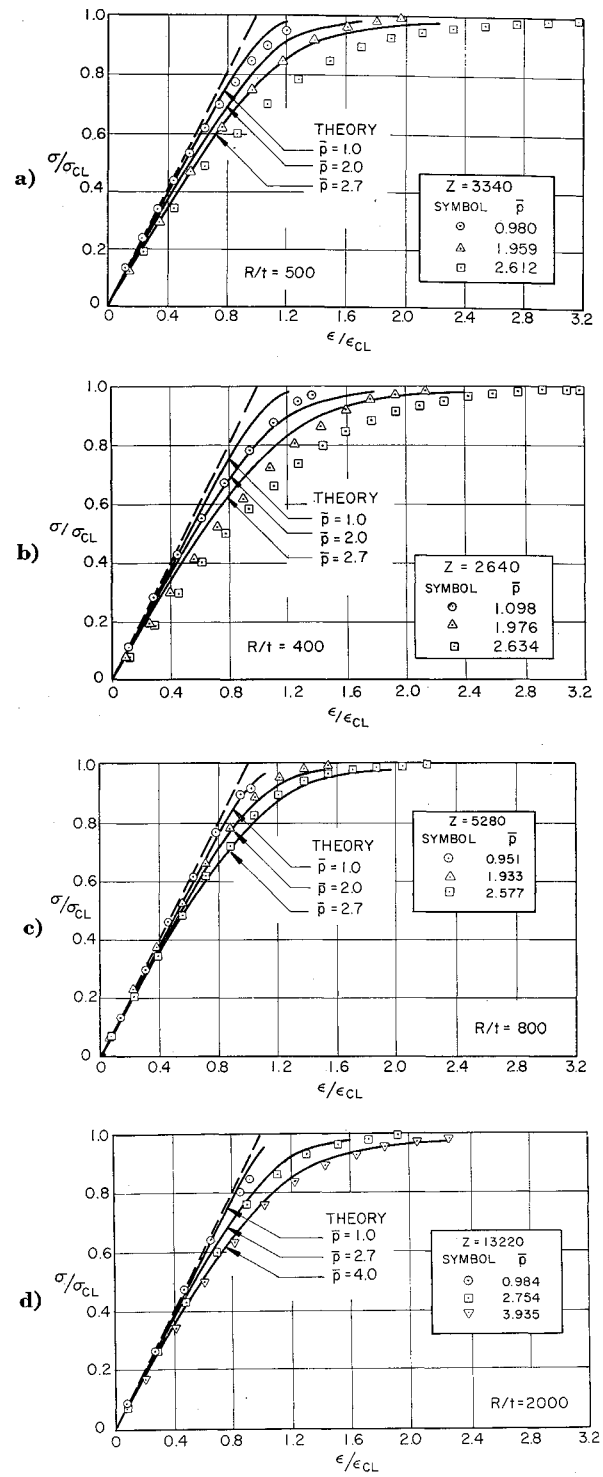

Fig. 4 Comparison of theoretical and experimental load-end shortening curves for pressurized cylinders.

Critical Axial Stress

The experimental results for critical axial stress as a function of internal pressure for the five skin thickness studies are plotted in Fig. 5 in terms of the two dimensionless parameters introduced by Lo, Crate, and Schwartz[3]: $\bar{\sigma}_{cr}$ and $\bar{p}$. Solid curves representing the approximate lower bound of the scatter band are also shown. It will be noticed that the general trend of variation of $\bar{\sigma}_{cr}$ with pressure is as predicted in Ref. 3, i.e., the tendency is for $\bar{\sigma}_{cr}$ to increase with increasing $\bar{p}$ and to reach a constant value at higher values of $\bar{p}$. As expected, since the influence of initial imperfections diminishes with increasing pressure, the experimental scatter is largest for very low pressures. This scatter appears to be dependent upon the end conditions, among other factors, since the two casting materials used, Cerrobend and Cerrolow, gave consistently different results. Generally, higher values of $\bar{\sigma}_{cr}$ were obtained for values of $\bar{p}$ up to 0.5 when Cerrolow was used. This tendency is illustrated in Fig. 6 by two series of tests on cylinders clamped in Cerrobend for the first series and in Cerrolow for the second series. The difference appears to result from the solidifying characteristics of the two alloys. Upon cooling, Cerrolow contracts slightly, whereas Cerrobend

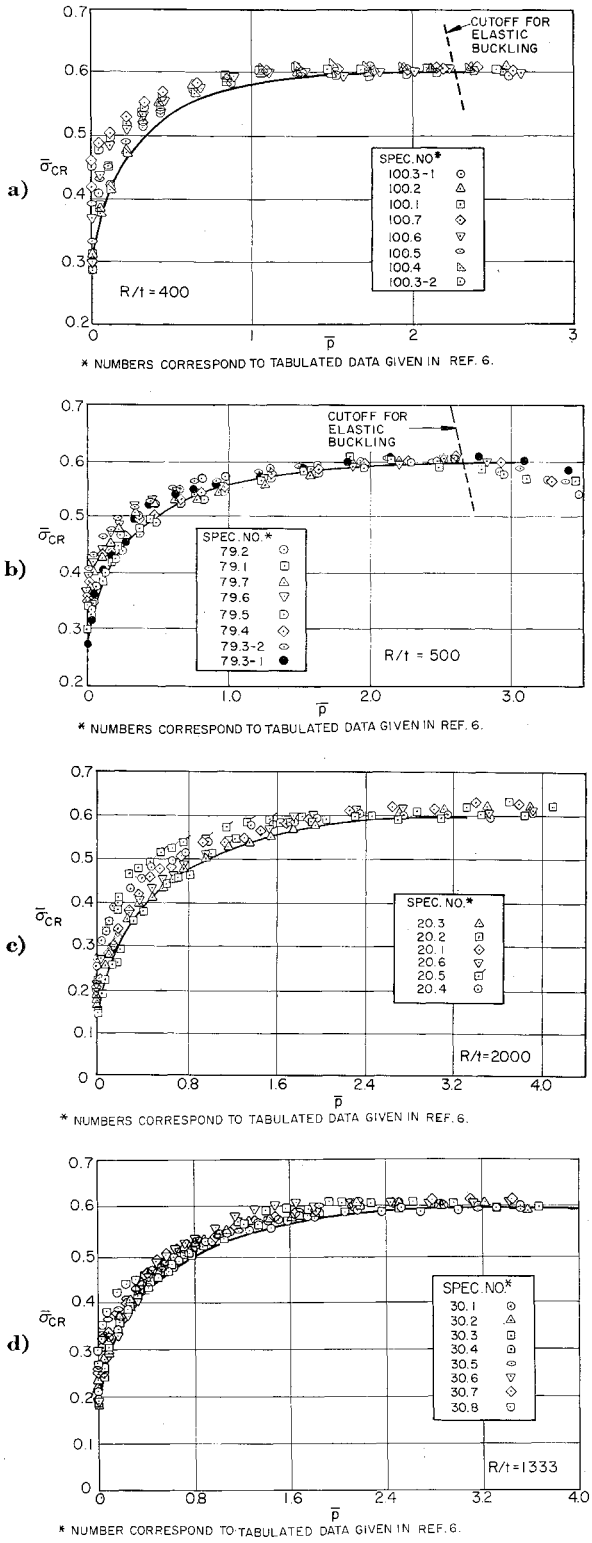

Fig. 5 Variation of axial-stress coefficient with internal pressure parameter.

expands approximately 25 times this amount of contraction. Thus the cylinders installed in Cerrobend had more eccentricity at the ends and, consequently, gave lower values of $\bar{\sigma}_{cr}$ until the internal pressure could overcome the influence of these initial imperfections. To illustrate the generality of this difference, the unpressurized results for both clamped conditions are compared in Fig. 7.

For comparison, the results for the various values of R/t curves representing the lower envelope of scatter of $\bar{\sigma}_{cr}$ vs $\bar{p}$

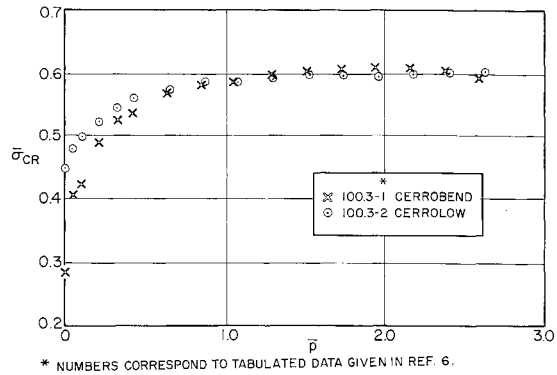

Fig. 6 Effect of end condition on axial-stress coefficients for pressurized cylinders.

are shown in Fig. 8. It appears that the buckling coefficients $\bar{\sigma}_{cr}$ are a function of the radius-thickness ratio for pressurized, as well as unpressurized, cylinders. However, in accordance with theory, the buckling coefficients converge to the classic value of $\bar{\sigma}_{cr}$, regardless of the values of R/t, in contrast to the results of Refs. 3–5.

The combined effects of axial load and internal pressure were not large enough for yielding to occur in the cylinders of smaller wall thickness, but the influence of plasticity was felt in the thicker cylinders. In Fig. 5b, plasticity near the end caps is illustrated by the drop-off of $\bar{\sigma}_{cr}$ for high values of $\bar{p}$. The cutoff line illustrated in Fig. 5b,

$$\bar{\sigma}_{cr} = 0.728\bar{\sigma}_{\text{prop limit}} - 1.174\bar{p}$$

was derived from a consideration of bending stresses at the ends of the cylinders and represents the combined axial stress and hoop stress that will cause the outer fibers to become plastic, based on a von Mises yield condition. The proportional limit has been used, rather than the yield stress, since $\bar{\sigma}_{cr}$ appears to drop off soon after the maximum stresses exceed this limit.

Comparison with Other Experimental Data

The data from the current tests have been summarized in Fig. 8, by curves representing the lower envelope of the experimental scatter. These curves have been used for comparison with the results from three earlier investigations. The data compiled by Dow and Peterson[1] for cylinders of 7075-T6 aluminum are plotted in Figs. 9a and 9b. In general, the results for these ring-stiffened cylinders are in good agreement with those for Mylar cylinders. The 7075-T6 aluminum results in Fig. 9a are somewhat higher since the length-radius ratio of the metal cylinders was 0.25 as compared to 2 for the Mylar cylinders. The range of pressures covered in these tests is limited. Tests covering a larger range of pressures are reported in Ref. 5, the results of which are plotted in Fig. 9c. The cylinders used in these tests were made from 18-8 half-

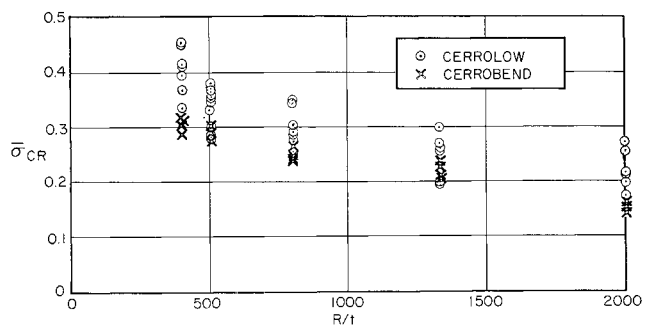

Fig. 7 Effect of end condition on axial-stress coefficients for unpressurized cylinders.

hard stainless steel that has a rather rounded stress-strain curve. The plasticity cutoff line derived from the proportional limit is illustrated in the figure. As in the case of Mylar, the buckling coefficients drop off steadily as the biaxial state of stress is increased beyond this limit. For low pressures, however, the results are in fair agreement with the present investigation. A high-strength stainless steel, 17-7 PH, was used in the investigation of Brown and Rea.[2] The results of these tests are plotted in Fig. 9d. At very low pressures, the influence of imperfections is evident, but, as the cylinder becomes stabilized by increased pressure, the results agree with those for Mylar. It is unfortunate that the tests were not extended to high values of $\bar{p}$, since the stresses were well below the elastic limit of the material.

One of the reasons for the discrepancy of other investigations thus appears to be the onset of plasticity resulting from clamped end-bending moments. The specimens used for the study of Ref. 1 differed from those of other investigations and of the present investigation in that they were ring-stiffened cylinders consisting of a test section and a buffer bay on either side of the test section. The rings helped to alleviate bending stresses due to end restraint and prevent premature buckling due to plasticity. In Refs. 1 and 8, Peterson and Dow concluded that the short buffer bays help to distribute the load and postpone premature buckling due to irregular stress dis-

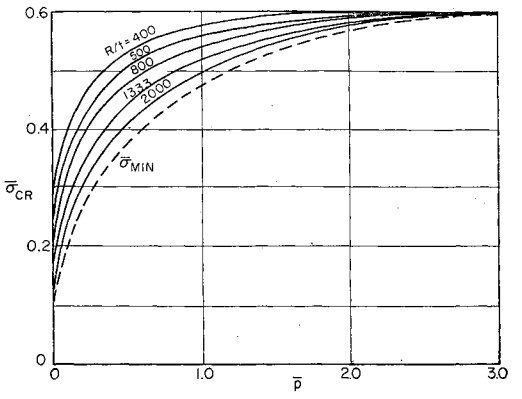

Fig. 8 Lower bound for variation of axial-stress coefficient with pressure parameter.

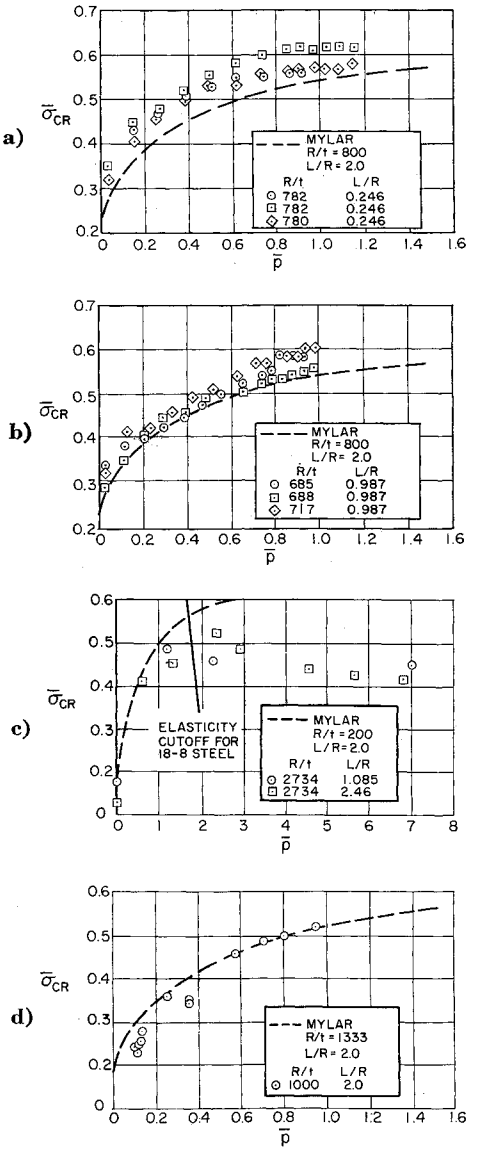

Fig. 9 Comparison of Mylar results with experimental data for other materials.

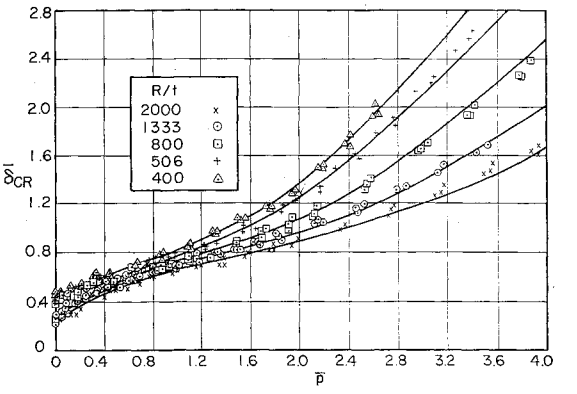

Fig. 10 Variation of critical end shortening parameter with internal pressure parameter.

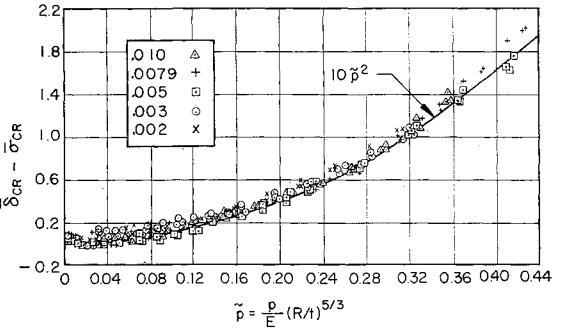

Fig. 11 Transformed data for variation of critical end shortening parameter with internal pressure parameter.

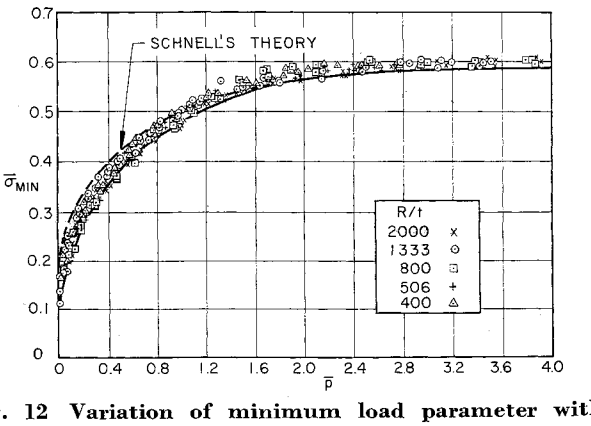

Fig. 12 Variation of minimum load parameter with internal pressure parameter.

tributions in the neighborhood of the ends. However, as can be seen from the comparison in the present paper, the results of Refs. 1 and 8 are not sensibly different from those obtained from specimens without buffer bays.

In some of the investigations, the buckling coefficients appeared to drop off prior to the predicted occurrence of plasticity (e.g., Fig. 9c). This discrepancy is suspected to be caused by plastic yielding of the material as the result of damage incurred during the preceding tests or, in the case of very thin specimens, during the fabrication process.

Critical End Shortening

Data for the axial deformation or end shortening at which buckling occurred were also taken from the load-deflection diagrams. These results are plotted in Fig. 10 in terms of nondimensional parameters similar to those used previously. The magnitudes of the deformation represent a measure of the axisymmetric radial deformations that occur prior to collapse, since the difference between the total end shortening and the compressive strain is equal to the nonlinear deformation associated with the rippling that occurs at high pressures. It was found by trial and error that plotting the strain difference ($\delta_{cr} - \bar{\sigma}_{cr}$) as a function of $(p/E)(R/t)^{5/3}$ (Fig. 11) eliminated the dependence upon radius-thickness ratios. It would be interesting to know if theoretical predictions bear any resemblance to the relation defined by this method of plotting.

Minimum Load

In addition to measurements of the critical load and end deformation, minimum load data were taken from the load-deflection diagrams. The minimum load, as used here, refers to the lowest load attained in the deformed equilibrium condition during the unloading process. The results for minimum load as a function of internal pressure for the five radius-thickness ratios are plotted in Fig. 12. The general trend of the variation of $\bar{\sigma}_{min}$ with the pressure parameter $\bar{p}$ is in accord with the dashed curve representing the values derived in Ref. 7. It is interesting to note, however, that the minimum values obtained here are less than those predicted; this would indicate that either the currently used large-deflection theory is not accurate enough for such large strains, or the current

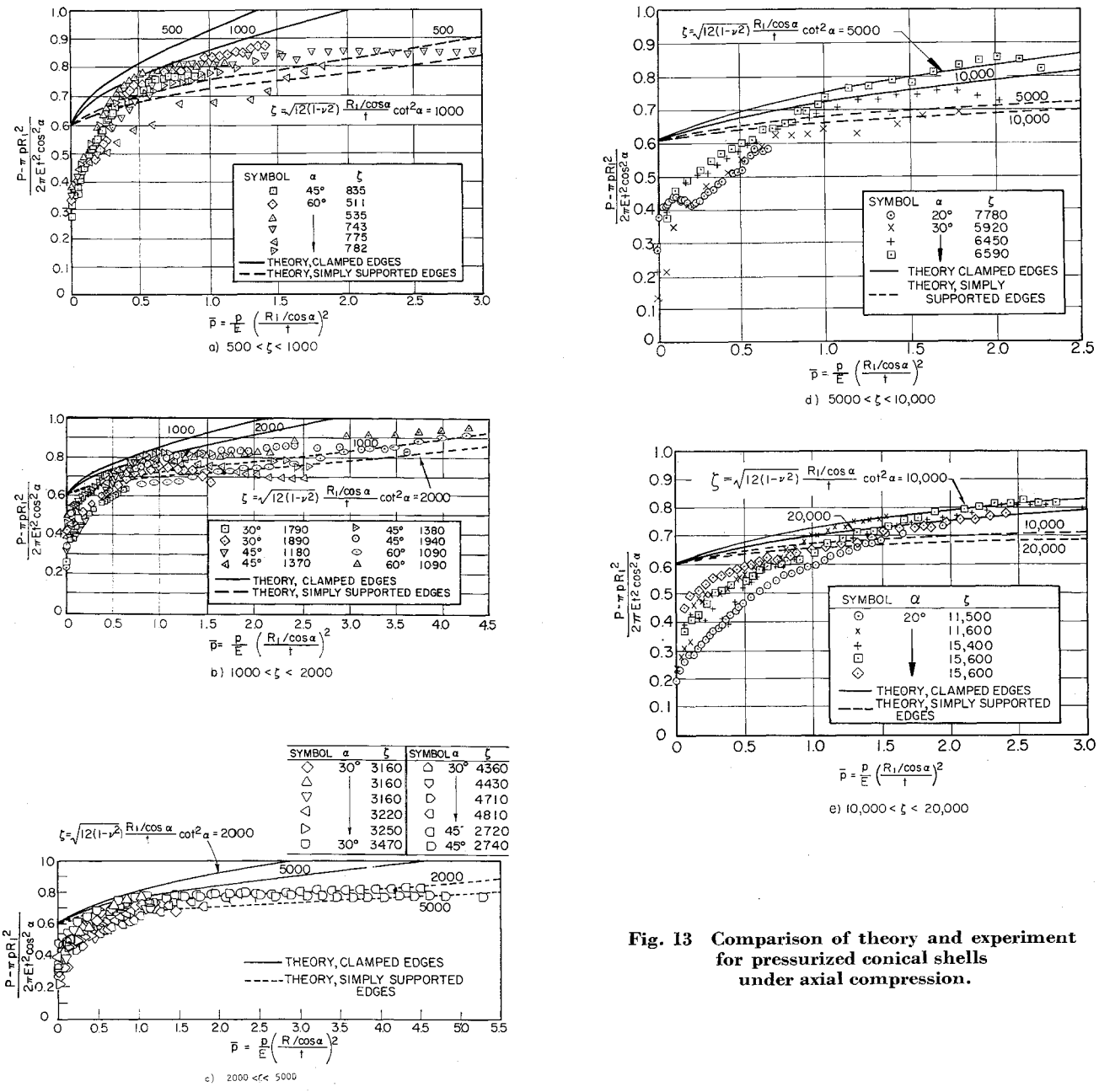

Fig. 13 Comparison of theory and experiment for pressurized conical shells under axial compression.

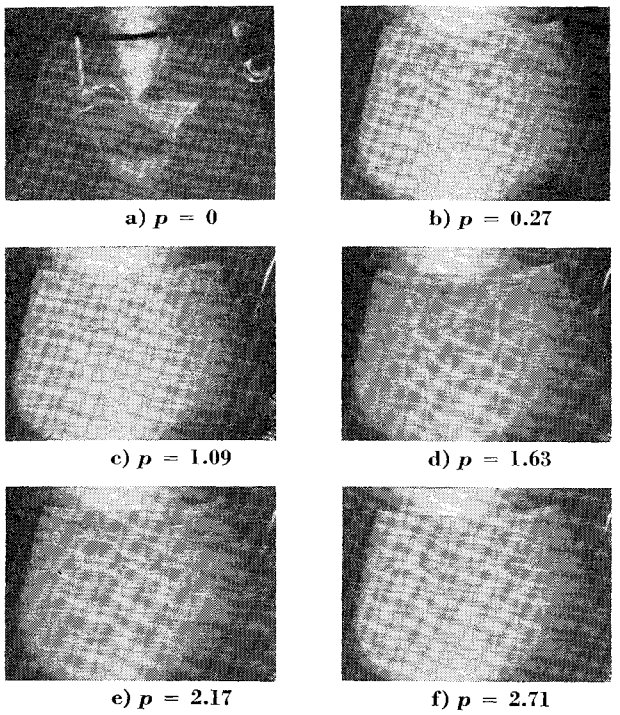

a) $p = 0$ b) $p = 0.27$ c) $p = 1.09$ d) $p = 1.63$ e) $p = 2.17$ f) $p = 2.71$

Fig. 14 Typical variation of axial compression buckle pattern with increasing internal pressure for conical shells.

solutions are not sufficiently accurate. As predicted by the theoretical solution of Ref. 9, for initially imperfect cylinders, there is little scatter in the measured values of the minimum stress coefficient, which is independent of the radius-thicknes ratio of the cylinders. The lower bound curve for $\bar{\sigma}_{\min}$ is included in Fig. 8. It is interesting to note that the lower envelope of the buckling coefficient curves appears to approach the curve for $\bar{\sigma}_{\min}$ as a limit, as the radius-thickness ratio increases.

Pressurized Truncated Cones under Axial Compression

Theoretical results for simply supported and clamped pressurized conical shells under axial compression[10] show that the axisymmetric buckling coefficient is a function of an internal pressure parameter and of a parameter containing the semivertex angle and the ratio of the small radius of curvature and the wall thickness. For sufficiently large pressures, i.e., for

$$\gamma = \{[3(1-\nu^2)]^{1/2}/2\}(p/E)[(R_1/\cos\alpha)/t]^2 > 1$$

the total axial load carrying capacity of the conical shell is given by

$$\frac{[3(1-\nu^2)]^{1/2}}{2\pi}\frac{P}{Et^2\cos^2\alpha} = (1+\gamma)(1+1.05^{-1/3})$$

where

$$\zeta = [12(1-\nu^2)]^{1/2}[(R_{1/\cos\alpha})/t]\cot^2\alpha$$

Calculated buckling patterns indicate that, as the pressure increases, the buckle deformations become confined to the small end of the cone, since this is the only part of the cone in compression.

The experimental results obtained from a relatively small number of tests investigating the predicted increase in net load carrying capacity, based on the small cross section of the cone, are compared with theoretical calculations in Fig. 13.§

§ These results also appear in Ref. 10.

It can be seen that the predictions of the small-deflection theory are qualitatively verified, in that cones with small-deflection theory are qualitatively verified, in that cones with lower values of the geometry parameter ζ appear to yield larger net-buckling-load coefficients as a function of the pressure parameter and, for sufficiently large pressures, the buckling-load coefficients increase linearly with pressure. It will be noted that the end fixity of most of the conical shells vary from fully clamped to simply supported as the pressure increases. The agreement between experimental results and the clamped end theoretical results becomes better as ζ increases. The results then indicate that the theoretical values for the simply supported boundary condition can be used as an estimate of the load carrying capacity of conical shells for the pressure parameter greater than unity.

The observed buckle patterns (Fig. 14) vary with internal pressure in a manner similar to that for cylinders. It follows then that a comprehensive experiment program should include an investigation of the effect of the ratio of the small radius of curvature to the wall thickness on cones having given values of the geometry parameter ζ.

It is also obvious from the results that the stress state becomes plastic near the ends of the specimens under sufficiently high pressures, as indicated by the drop-off in net buckling load for some specimens. Thus, the benefits of pressurization are limited by the onset and effects of plasticity which are dependent on the plastic behavior of the particular material used. The test results of Ref. 2 for high-strength stainless-steel specimens are in good agreement with those of the present investigation but do not cover a large enough range of pressure to verify the theoretical increase in net load carrying capacity over that for the cylinder for large pressures. It has been noted, however, both in the present results and in those of Ref. 2, that cones appear to be relatively stronger than cylinders in the low-pressure range. The results of Ref. 11 appear to be considerably lower than those of the present paper. It is difficult to effect a direct comparison since the test results tabulated in Ref. 11 contradict the results given graphically. Since the load level never reached the theoretical value, even at relatively high pressure, the cones are concluded to have been of inferior construction.

Concluding Remarks

The results of the present program qualitatively verify the behavior of elastic, pressurized cylinders under axial compression predicted in Refs. 3 and 7 in that the load carried by the cylinder in addition to that carried by internal pressure increases to the value given by small-deflection theory for unpressurized cylinders. The variation of the net load with internal pressure has been found to depend on the radius-thickness ratio of the cylinder, and curves suitable for design have been obtained.

The predicted load-pressure variation of Ref. 3, based on a transfer-of-energy concept due to Tsien and calculated for an infinitely rigid testing machine, overestimates the effect of pressure. It is interesting to note that the results of most of the investigators, obtained from specimens of different materials and with different testing machines, are similar. The results show that the conclusion reached in Ref. 3 and perpetuated in Refs. 4 and 5 (that the buckling stress of a pressurized cylinder is equal to the sum of the buckling load of the unpressurized cylinder and an increment due solely to pressure) is coincidental and that this concept should be abandoned.

For sufficiently high pressures, the behavior of the cylinders prior to buckling is in good quantitative agreement with calculations based on linearized axisymmetric large-deflection theory (the beam column on an elastic foundation), although some unexplained anomalies have been found for the thicker cylinders tested. At some critical value of strain, dependent on the pressure and the radius-thickness ratio, the cylinder

snaps into a diamond-shaped buckle mode and the load decreases. Measured load-deflection curves show that the presently accepted solution of the large-deflection equations for diamond-shaped deformations is inaccurate. Whether this is a result of limitations of the equations or to limitations of their solution is uncertain. It is also uncertain whether or not it would be necessary to solve the large-deflection equations for a finite cylinder to obtain good agreement between theory and experiment.

Experimental buckling loads for conical shells are in relatively good agreement with those based on small-deflection theory for sufficiently high pressures, but indicate that the end-support condition may be more important than for cylinders. Insufficient data are available to enable design curves to be recommended for the region of low-pressure parameter.

One problem for future experimental investigations is the effect of length on the results for cylinders (all results were obtained for cylinders having a constant length and radius). Much additional data is needed for cones for varying values of small radius-thickness ratio, semivertex angle, and length. Finally, the effects of plasticity need to be explored since this factor places limits on the applicability of the present results to metal structures.

References

[1] Dow, M. B. and Peterson, J. P., "Bending and compression tests of pressurized ring-stiffened cylinders," NASA TN D-360 (April 1960).

[2] Brown, J. K. and Rea, R. H., "The elastic stability of thin-walled pressurized conical shells under compression and compression-bending interaction," M. S. Thesis, Institute of Technology (Air University), Wright-Patterson Air Force Base (August 1960).

[3] Lo, H., Crate, H., and Schwartz, E. B., "Buckling of thin-walled cylinders under axial compression and internal pressure," NACA Rept. 1027 (1951).

[4] Fung, Y. C. and Sechler, E. E., "Buckling of thin-walled circular cylinders under axial compression and internal pressure," J. Aeronaut. Sci. **24**, 351–356 (1957).

[5] Harris, L. A., Suer, H. S., Skene, W. T., and Benjamin, R. J., "The stability of thin-walled unstiffened circular cylinders under axial compression including the effects of internal pressure," J. Aeronaut. Sci. **24**, 587–596 (1957).

[6] Seide, P., Weingarten, V. I., and Morgan, E. J., "Final report on the development of design criteria for elastic stability of thin shell structures," Space Technology Labs. Rept. STL/TR-60-0000-19425 (December 1960).

[7] Schnell, W., "Zur Stabilitat Dunnwandiger Langsgedruckter Kreiszylinderschalen bei Zusatzlichem Innendruck," *Proceedings of the International Union of Theoretical and Applied Mechanics Symposium on the Theory of Thin Elastic Shells* (North-Holland Publishing Co., Amsterdam, 1960).

[8] Peterson, J. P. and Dow, M. B., "Structural behavior of pressurized ring-stiffened, thin-wall cylinder subjected to axial compression," NASA TN D-506 (1960).

[9] Donnell, L. H. and Wan, C. C., "Effect of imperfections on buckling of thin cylinders and columns under axial compression," J. Appl. Mech. **17**, 73–88 (March 1950).

[10] Seide, P., "On the stability of internally pressurized conical shells under axial compression," *Proceedings of the Fourth U. S. National Congress of Applied Mechanics* (University of California, Berkeley, Calif., 1962).

[11] Lofblad, R. P., "Stability of thin-walled cylinders and cones with internal pressure under axial compression," Massachusetts Institute of Technology, TR 25-29, Office of Naval Research Contract No. Nonr-1841 (22) (May 1959).